Figure 1 shows the range and endurance of a number of aircraft plotted vs the approximation of Eq. (15) for various cruise speeds. Aircraft shown include the F/A-18, P-3, S-3, Global Hawk, Harrier, E-2C, and C-2, selected because both range and loiter information are available in public sources.[2] Also included is the notional light twin described earlier. Figure 1 shows a fairly good correspondence, with the given data points lying fairly near their equivalence line for their cruise speed.

The only exception is the Global Hawk. (See data point with greatest range and loiter.) Global Hawk flies at extreme altitude, where its maximum speed and its stall speed are almost the same, and so it cannot slow down for more optimal loiter. Its loiter time is just slightly greater than range divided by cruise speed, without the 14% adjustment suggested herein.

Summary

A relationship between range and endurance was derived, based on the Breguet range and loiter equations. Given a known aircraft range and the cruise speed, equivalent loiter time can be estimated by a simple and useful rule of thumb: Loiter time equals range divided by cruise velocity, increased 14%.

Despite different derivations, this approximation can be used for both jets and propeller aircraft. Checks of this method were made that seem to indicate reasonable prediction of loiter time based on publicly available data, with results typically within 5% of the correct values.

References

[1]Raymer, D., *Aircraft Design: A Conceptual Approach*, 3rd ed., AIAA, Washington, DC, 1999.

[2]Taylor, J., *Jane's All the World Aircraft*, Jane's, London, 2000.

[3]Raymer, D., "Enhancing Aircraft Conceptual Design using Multidisciplinary Optimization," Ph.D. Dissertation, Dept. of Aeronautics, Swedish Royal Inst. of Technology, Stockholm, May 2002.

Viscous Flow Solutions over CN-235 Cargo Aircraft

Murat Uygun*
Turkish Air Force Academy, 34149 Istanbul, Turkey
and
Ismail H. Tuncer†
Middle East Technical University, 06531 Ankara, Turkey

Introduction

THE cost of predictions from computational fluid dynamics (CFD) is continually decreasing relative to costs associated with wind-tunnel experiments. Flow solutions computed with CFD codes present detailed flowfield information, which might be too expensive to obtain in a wind tunnel. Consequently, CFD methods are becoming more popular and are being used for complementing experimental studies to decrease the number of wind-tunnel measurements. Aircraft companies rely heavily on the CFD methods in the preliminary design of a new aircraft or in the modification of an existing one.

Received 7 April 2003; presented as Paper 2003-3661 at the 21st Applied Aerodynamics Conference, Applied computational aerodynamics with validation, Orlando, FL, 23 June 2003; revision received 22 January 2004; accepted for publication 23 January 2004.

*Research Engineer, Department of Aeronautical Engineering; uygun@ae.metu.edu.tr. Member AIAA.

†Associate Professor, Department of Aerospace Engineering; tuncer@ae.metu.edu.tr. Member AIAA.

Table 1 Aircraft model data

Parameter	Value
Overall length, m	21.353
Full span, m	25.81
Root chord, m	3.0
Wing mean chord, m	2.62
Wing gross area, m	59.1
Wing incidence angle, deg	3
Wing airfoil	$NACA65_3$-218
Horizontal and vertical tail airfoils	$NACA64_1$-012

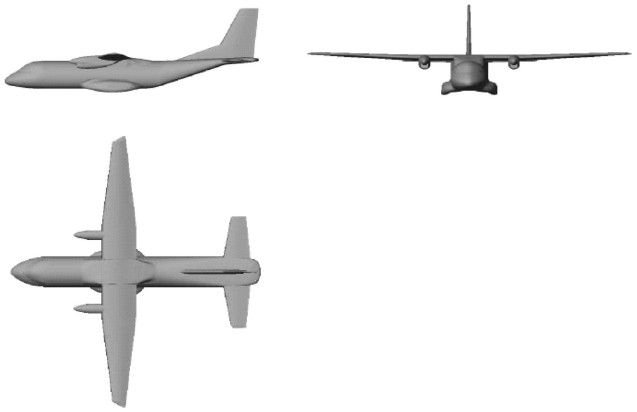

Fig. 1 Aircraft model geometry.

The CN-235 aircraft (Fig. 1 and Table 1) is a twin turboprop tactical transport aircraft having a maximum cruising speed of 455 km/h (Ref. 1). It was initially designed and built through cooperation between Construcciones Aeronuticas SA (CASA) of Spain and Dirgantara Indonesia (IPTN). Later, CASA developed its own versions.

It has been built by Turkish Aerospace Industries (TAI) of Turkey under production license by CASA for several years. It has a reputation for mission versatility, minimum support requirements, and reliable operation in a wide range of environments. It has been modified for both civilian and military purposes, and has gained civil certification by safety bodies in many countries. Modified versions of the aircraft are in military service in more than 20 countries, including Turkey.

In the past, CFD methods have been employed for the aerodynamic analysis of the CN-235 aircraft. Karaagac[2] used Advanced Aircraft Analysis (AAA) software[3] (ver. 2.2) to compute the aerodynamic characteristics of the CN-235 aircraft. AAA is based on empirical methods for airplane design, airplane flight dynamics and automatic flight controls, and airplane aerodynamics and performance. It is widely used for preliminary design, stability, and control analysis of a new and existing airplane. Bahar et al.[4] obtained inviscid flow solutions for CN-235 aircraft using the CFD-FASTRAN flow solver[5] (ver. 2.2) with unstructured grids. Kurtulus recently computed viscous and inviscid flows over CN-235 at cruise, landing, and takeoff conditions using the VSAERO software (ver. 6.2),[6,7] which is a panel-based potential flow solver with viscous–inviscid interactions.

In this study, viscous flows over CN-235 cargo aircraft are computed at cruise conditions and at angles of attack ranging from 0 to 5 deg by the use of the CFD-FASTRAN Navier–Stokes solver. Computations are performed on a Pentium III-based personal computer with a 1-Gb memory. Grid sensitivity and verification studies are performed on the clean-wing configuration (Fig. 2). Inviscid and viscous flow solutions with available turbulence models over the full aircraft are compared at a range of incidence angles. Computed lift and drag values are also compared with semi-empirical and numerical data available in the literature. It is shown that viscous flow solutions provide valuable aerodynamic data, which may

be used to determine and/or alter the aerodynamic characteristics of the aircraft.

Numerical Tools

In this study, CFD-FASTRAN Navier–Stokes solver (ver. 2.2) and the CFD-GEOM grid generation software[8] (ver. 5) are used to obtain viscous and inviscid flow solutions on structured, multiblock grid system.

CFD-FASTRAN is a Navier–Stokes solver based on a cell-centered finite volume discretization. Flowfields may be discretized with structured, unstructured, or hybrid grids. First- and higher-order accurate inviscid fluxes may be computed with Roe's flux difference splitting scheme[9] and Van Leer's flux vector splitting scheme.[10] CFD-FASTRAN has an algebraic (Baldwin–Lomax[11]) and two-equation (k–ε model[12] and k–ω model[13]) turbulence models.

Computational grids are generated with the CFD-GEOM grid-generation software. CFD-GEOM can generate the multiblock structured and unstructured grids with point match interface, overset (chimera) grids, and hybrid grids (structured–unstructured grids). For structured grids, grid orthogonality at the wall boundaries may be enforced, and grid quality may be improved with elliptic smoothers. In generating unstructured grids, CFD-GEOM provides an automatic and controllable surface triangulation and tetrahedral volume grid-generation algorithms via the advancing front technique. However, it does not provide a user control over the grid spacing in the direction normal to the wall boundaries. The grid resolution in the boundary layers may, therefore, be poor, and unstructured grids may not be employed in viscous flow computations. Overset (overlapping) grids also provide simplicity in grid generation around complex geometries. However, similar grid densities have to be provided at the overlapping intergrid boundaries.

Results and Discussion

In this study, inviscid and turbulent flow solutions were obtained for clean-wing and full-aircraft configurations. Structured, overset, hybrid, and unstructured grids were employed in the solutions. All flows were computed at the cruise condition of the aircraft [at Mach number 0.39 and at an altitude of 15,000 ft (4600 m)]. The flow cases studied are listed in Table 2. Inviscid and viscous results presented here were computed on structured and unstructured grids only. A fully turbulent flow is assumed for viscous flows.

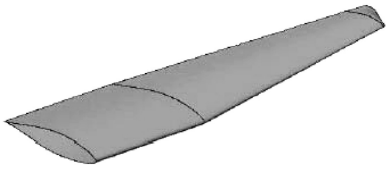

Fig. 2 Clean-wing model geometry.

Table 2 Flow cases considered in this study

Performance	Clean wing	Aircraft
Inviscid flow	√	√
Viscous flow	√	√
Structured grid	√	√
Unstructured grid	√	——
Hybrid grid	——	√
Overset grid	√	√

The origin of the coordinate system used in this study is located at the nose of the aircraft, on the symmetry axis. The x coordinate extends downstream in the chordwise direction, and the z coordinate extends along the spanwise direction. The computational grids were generated for the one-half configuration due to the symmetry in the configuration, and the symmetry boundary condition was applied. Wall boundary conditions were implemented to the solid boundaries. Inflow/outflow boundary conditions, which are based on the Riemann invariants, were implemented to the rest of the boundaries.

Inviscid fluxes in viscous and inviscid flows were evaluated by the Roe flux differencing scheme[9] and/or the Van Leer flux vector splitting scheme.[10] In the numerical solutions, the fully implicit time integration scheme with third-order spatial accuracy is used. The Courant–Friedrichs–Lewy (CFL) number was varied between 50 and 100, except for the viscous computations around the aircraft configuration, for which it was set to 5. The sensitivity of the viscous flow solutions to the turbulence models was established by computing the viscous flows over the clean-wing configuration with the Baldwin–Lomax, k–ω, and k–ε models. The optimum grid distributions on the wing surface and the location of the outer boundary were established in earlier studies for grid-independent solutions.[5,14] Computations were performed in double precision on a personal computer with a Pentium III, 450-MHz processor and 1-Gb memory operating on Windows NT.

$y_1^+ = 1$ was used for Baldwin–Lomax and k–ω models, and $y_1^+ = 40$ for k–ε model, which implements the law of the wall explicitly. A $147 \times 167 \times 30$ size grid was used, and a typical solution required 380 Mb of memory and took about 50 h of CPU time.

Pressure distributions on the wing computed with each turbulence model and for an inviscid flow are shown in Fig. 3. As shown, all of the models predict about the same pressure variation as the inviscid flows, except k–ω model, which slightly differs from the others near the upper wing tip region and at the stagnation point. The computed lift forces are given in Table 3. The k–ω model yields a lift force about 2.2% smaller than the others. The total drag force and viscous drag component for the different y_1^+ locations are given in Table 3. The drag force based on the Baldwin–Lomax model is about 16% greater than that of the k–ε model, and 17% smaller than that of the k–ω model. It is also observed that the drag forces based on each turbulence model decrease as much as 15% as the y_1^+ values are increased beyond the proper values.

The variation of lift, drag, and pitching moment coefficients with respect to angle of attack and the drag polar are given in Fig. 4. The lift and the pitching moment coefficients based on all of the

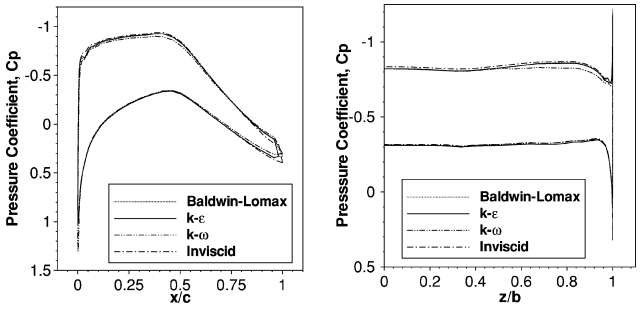

Fig. 3 Pressure distribution along the chord at the 75% span location and along the span at the midchord, $P = 57{,}207$ Pa; $M = 0.39$; and $\alpha = 3$ deg.

Table 3 y_1^+ Turbulence model sensitivity study, total and viscous aerodynamic drag forces at $\alpha = 3$ deg

y_1^+ value	Baldwin–Lomax D, N			k–ε D, N			k–ω D, N		
	L	Total	Viscous	L	Total	Viscous	L	Total	Viscous
1	92,359	3,271	1,062		——	——	90,387	3,943	1,132
5	92,013	3,172	1,117		——	——	91,409	3,357	982
40		——	——	92,380	2,752	909		——	——
100		——	——	92,555	2,685	870		——	——
200		——	——	92,625	2,665	855		——	——

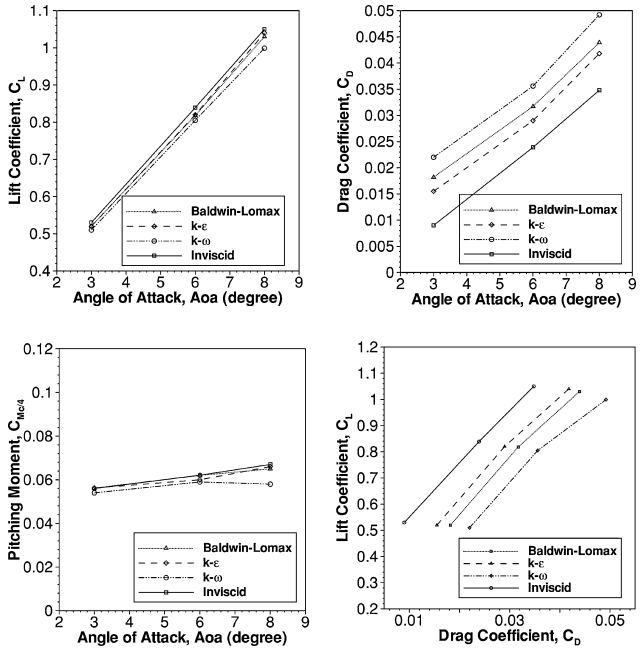

Fig. 4 Variation of the aerodynamic forces and moments for the clean-wing.

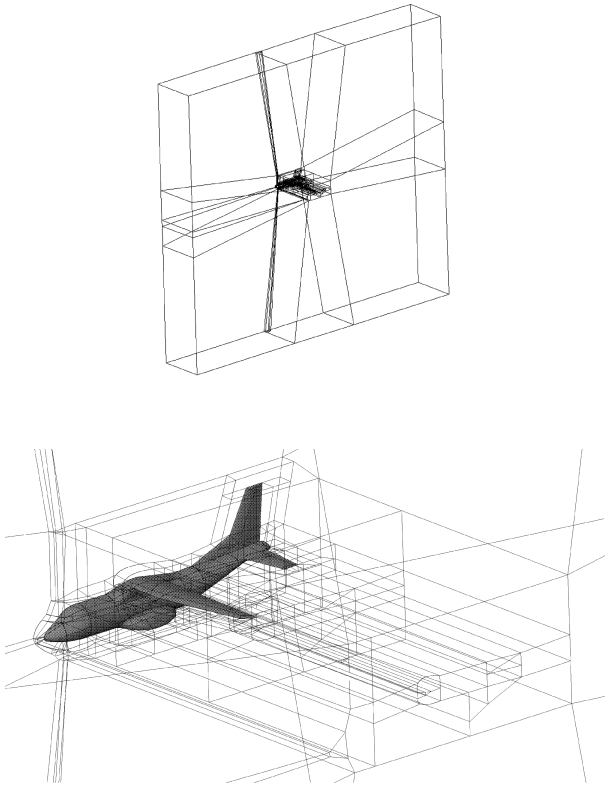

Fig. 5 Block layout of the multiblock structured grid around the aircraft.

turbulence models agree reasonable well among themselves and with the inviscid flow prediction. Yet, as the angle of attack increases, the k–ω model predicts slightly lower values. The pitching moment values at the mean quarter-chord increase slightly with the angle of attack, which indicates that the aerodynamic center is slightly off of the quarter-chord location. Similarly, large differences in drag predictions are observed at $\alpha = 5$ deg as well.

Because a viscous grid could not be built around the nacelle, it was removed from the aircraft configuration in the analysis of the full aircraft. A multiblock structured grid of 122 blocks was then created around the aircraft (Fig. 5). Degenerate blocks where one

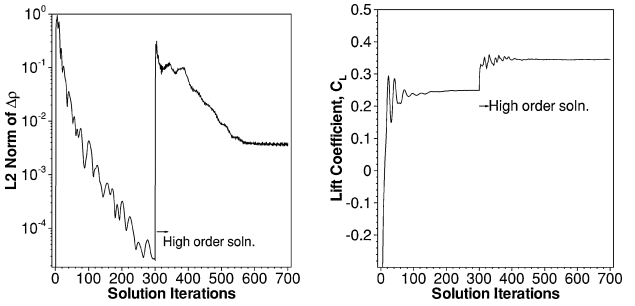

Fig. 6 Convergence and lift histories for the inviscid flow computation at $\alpha = 0$ deg.

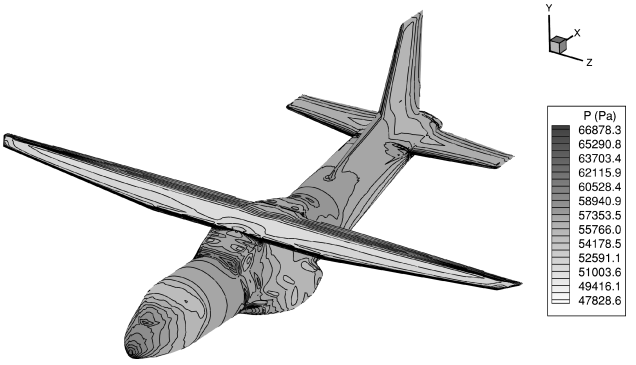

Fig. 7 Inviscid pressure distribution on the aircraft, $P = 57{,}207$ Pa; $M = 0.39$; and $\alpha = 0$ deg.

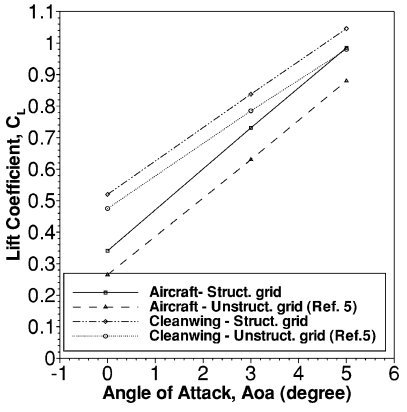

Fig. 8 Lift forces for inviscid flows on the aircraft and on the clean wing at $\alpha = 0$, 3, and 5 deg.

of the block edges collapses to a point were avoided to improve the convergence of the solution. The grid generation process took about four work weeks. The same multiblock topology was used to generate both inviscid and viscous grids by adjusting the grid spacing normal to the wall. The inviscid and viscous grids had about 1.8 and 2.3 million hexahedrals, respectively.

First, inviscid flows are computed at 0-, 3-, and 5-deg angles of attack. The solution required 686 Mb of RAM and about 200 h of CPU time. Figure 6 shows the convergence history of the inviscid solution and the lift history at $\alpha = 0$ deg. The computed pressure distribution is given in Fig. 7. The lift computed on the full aircraft is found to be about 35% less than that on the clean wing at $\alpha = 0$ deg and 6% less at $\alpha = 5$ deg, as shown in Fig. 8. The reduced lift is attributed to the 10% reduction on the wingspan of the aircraft compared to the wingspan of the clean-wing model and the aircraft fuselage interference. The negative incidence angle of the horizontal tail also adds to the loss of lift. Bahar's inviscid computations on unstructured grids[4] yield smaller lift values than the present computations on structured grids, which may be attributed to the finer resolution of the flowfield with structured grids.

For the viscous flow solutions with the k–ε turbulence model, the grid blocks were refined at the walls to provide a sufficient

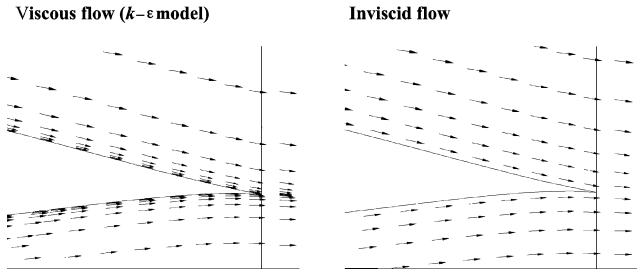

Fig. 9 Velocity fields at 95% span, $P = 57{,}207$ Pa; $M = 0.39$; and $\alpha = 5$ deg.

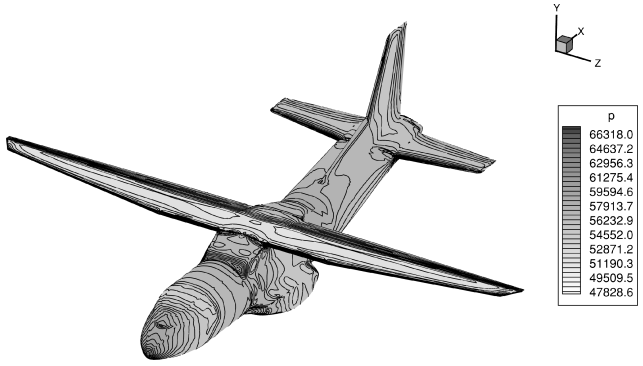

Fig. 10 Pressure distribution on the aircraft for the viscous flow, $P = 57{,}207$ Pa; $M = 0.39$; and $\alpha = 0$ deg.

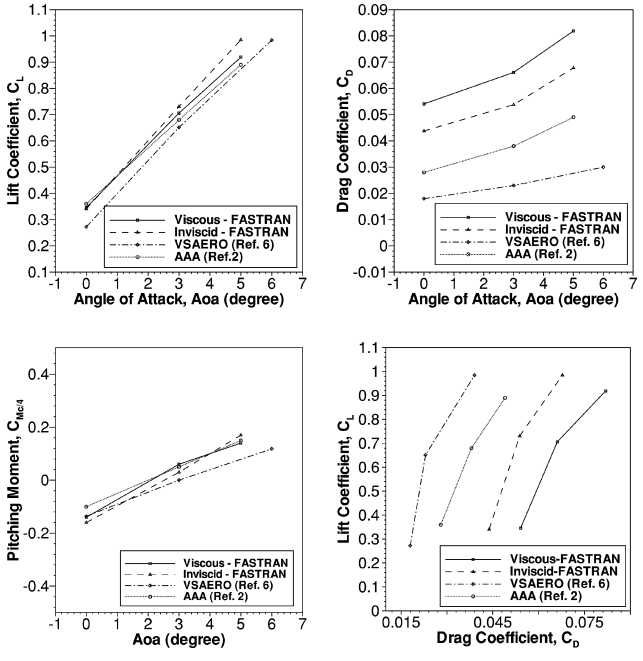

Fig. 11 Variation of the aerodynamic forces and moments for the aircraft.

grid resolution in boundary layers. In the computations, the double-precision version of the flow solver was used, and the CFL number was set in the 1–5 range. The computations took about 300 h of CPU time. Investigation of the viscous flowfield shows that as opposed to the computed flow over the clean-wing configuration,[14] the viscous flow over the aircraft configuration does not produce any flow separation at 95% wingspan (Fig. 9).

The computed pressure distribution at $\alpha = 0$ deg is given in Fig. 10. The integrated aerodynamic loads are given in Fig. 11. It is observed that in the viscous flow solutions the lift is reduced by about 3.6% at $\alpha = 3$ deg and 7% at $\alpha = 5$ deg, which may be attributed to

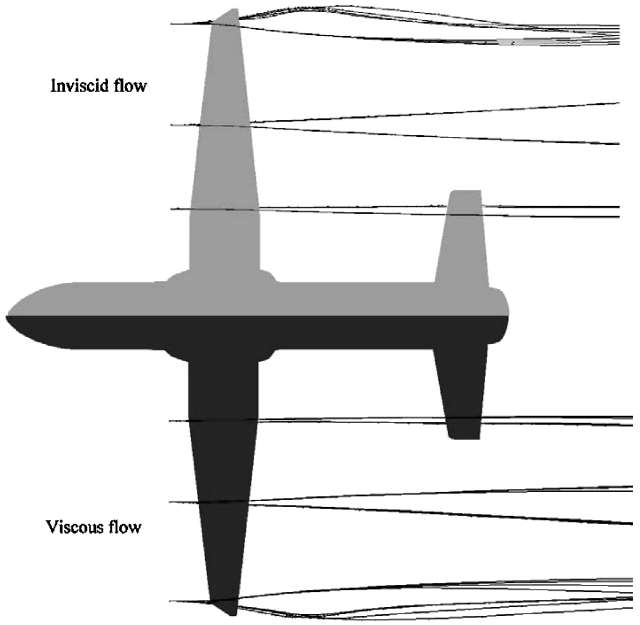

Fig. 12 Particle traces for the inviscid and viscous (with k–ε model) flows, $P = 57{,}207$ Pa; $M = 0.39$; and $\alpha = 5$ deg.

the viscous effects. The viscous drag force is about 18% higher than that of the inviscid flow solution. The aerodynamic loads computed by AAA and VSAERO underpredict those of the CFD-FASTRAN solutions, but they all show the same trend. The predictions of the pitching moment at the mean quarter-chord agree well. The particle traces at the tip region do not show a significant variation than that of the inviscid flow (Fig. 12). It again suggests that the tip vortex is pressure driven and can be captured in inviscid flows.

Conclusions

In this study, low-speed, viscous flows over the CN-235 cargo aircraft were computed with the CFD-FASTRAN Navier–Stokes flow solver. Sensitivity studies of y_1^+ were first performed on the clean-wing configuration. Inviscid and viscous flows were then computed on the aircraft configuration at the cruise condition. It is shown that viscous flow analysis for a full-aircraft configuration is now feasible on today's powerful personal computers. Although the CFD-FASTRAN has proven to be a viable software in the computation of flows over complex aircraft configurations, the unstructured grid methodology in CFD-GEOM lacks the effective user-level controls to provide sufficient grid resolution in the boundary layers. Viscous flows were only studied by the use of the multiblock structured grids, which are highly time consuming to produce over complex aircraft configurations. The computed lift and moment coefficients based on viscous flows agree well with the inviscid flow predictions, as well as the panel code and the semi-empirical predictions. Drag values based on the available turbulence models yielded slightly different values, which need to be compared with the experimental data when they become available for further assessment.

Acknowledgment

The authors gratefully acknowledge the support provided by ASELSAN, Inc., Ankara, Turkey.

References

[1]*Jane's All the World's Aircraft*, Jane's Information Group, Surrey, England, U.K., 1991.

[2]Karaagac, C., "The Aerodynamics, Flight Mechanics and Performance Predictions for a Medium Range Cargo Aircraft," M.S. Thesis, Dept. of Aerospace Engineering, Middle East Technical Univ., Ankara, Turkey, Nov. 1998.

[3]"Advanced Aircraft Analysis Software," Design, Analysis, and Research Corp., KS.

[4]Bahar, C., Alemdaroglu, N., Ozyoruk, Y., and Temel, E., "Euler Solutions for a Medium Range Cargo Aircraft," *Journal of Aircraft*, Vol. 40, No. 2, 2003, pp. 393–395.
[5]"CFD-FASTRAN User Manual," ver. 2.2, CFD Research Corp., Huntsville, AL, 1998.
[6]Kurtulus, D. F., "Aerodynamic Analysis of a Medium Range Cargo Aircraft Using a Panel Method," M.S. Thesis, Dept. of Aerospace Engineering, Middle East Technical Univ., Ankara, Turkey, Jan. 2002.
[7]Nathman, J., "VSAERO User's Manual," Analytics Methods Inc., Redmond, WA, 1982.
[8]"CFD-GEOM User Manual," ver. 5, CFD Research Corp., Huntsville, AL, 1998.
[9]Roe, P. L., "Approximate Riemann Solvers, Parameter Vectors and Difference Schemes," *Journal of Computational Physics*, Vol. 43, No. 2, 1981, pp. 357–372.
[10]Van Leer, B., "Flux-Vector Splitting for the Euler Equations," *Lecture Notes in Physics*, Vol. 170, Springer-Verlag, NY, 1982, pp. 507–512.
[11]Baldwin, B. S., and Lomax, H., "Thin Layer Approximation and Algebraic Model for Separated Flows," AIAA Paper 78-257, Jan. 1978.
[12]Speziale, C., Abi, R., and Anderson, E., "A Critical Evaluation of Two-Equation Models for Near-Wall Turbulence," AIAA Paper 90-1481, Jan. 1990.
[13]Wilcox, D. C., "A Half Century Historical Review of the k–ω Model," AIAA Paper 91-0615, Jan. 1991.
[14]Uygun, M., and Tuncer, I. H., "A Computational Study of Subsonic Flows over a Medium Range Cargo Aircraft," AIAA Paper 2003-3661, June 2003.

Effects of Flow Separation on Aerodynamic Loads in Linearized Thin Airfoil Theory

A. Khrabrov*
TsAGI, Russia
and
M. Ol†
U.S. Air Force Research Laboratory, Wright–Patterson Air Force Base, Ohio 45433-7542

Introduction

In various problems of modeling steady and unsteady aerodynamic loads, it is useful to know the explicit dependence of the loads on the airfoil upper-surface separation point location, for example, see Ref. 1. We consider an approach based on classical thin airfoil theory, for symmetrical airfoils at small angles of attack, that is, inclined flat plates.[2–4] A separated region in an ideal fluid is modeled as a semi-infinite zone of uniform pressure with Kirchhoff's free streamline boundaries, originating from a prescribed location on the airfoil upper surface and from the trailing edge. A closed-form solution for lift and pitching moment coefficient is obtained by assuming small angles of attack and thin separated regions, thus allowing linearization.

The linear solution is obtained in singular integral form.[5] It is then compared to the Chaplygin and Lavrentiev classical solution[6] and an XFOIL solution[7,8] for a NACA 0012 airfoil.

Received 14 October 2003; revision received 19 January 2004; accepted for publication 20 January 2004.

*Chief, Unsteady Aerodynamics Branch, Central Aerohydrodynamics Institute; khrabrov@postman.ru.
†Aerospace Engineer, Air Vehicles Directorate, Aeronautical Sciences Division; Michael.Ol@wpafb.af.mil. Member AIAA.

Linear Thin Airfoil Theory with Flow Separation

The flowfield in the physical plane is shown in Fig. 1a. To make the problem dimensionless, the airfoil has unit chord and the velocity at infinity is a vector of unit magnitude. Free streamlines emanate from the airfoil trailing edge and the upper-surface separation point. On these streamlines, the pressure is uniform and equal to the value at infinity. The difficult task of determining the geometry of these streamlines is circumvented in the linear approximation, where the respective boundary conditions can be enforced on the Ox axis.

Because the vorticity vanishes everywhere except on the airfoil boundary and the free streamlines, the velocity field has a potential. When the boundary-value problem is posed in terms of the disturbance potential φ, the boundary conditions become no through-flow on the wetted portion of the airfoil, uniform pressure on the boundaries of the separated zone (equivalent to zero streamwise component of disturbance velocity), finite velocity at both separation points, and the disturbance potential decaying to zero at infinity:

$$\begin{aligned}
\triangle\varphi &= 0 \\
\varphi_y &= V(x), \qquad 0 < x < x_s, \qquad y = +0 \\
\varphi_y &= V(x), \qquad 0 < x < 1, \qquad y = -0 \\
\varphi_x &= 0, \qquad x_s < x < \infty, \qquad y = +0 \\
\varphi_x &= 0, \qquad 1 < x < \infty, \qquad y = -0 \\
\varphi_x &< \infty, \qquad x = x_s, \qquad y = +0 \\
\varphi_x &< \infty, \qquad x = 1, \qquad y = -0 \\
\varphi &\to 0, \qquad x^2 + y^2 \to \infty
\end{aligned} \tag{1}$$

$V(x)$ is known on the wetted portion of the airfoil, as a function of angle of attack and airfoil shape. Appealing to complex variables theory, we introduce the complex flow potential W, and seek the complex conjugate disturbance velocity $\mathrm{d}W/\mathrm{d}z = U - iV$, where $U = \varphi_x$ and $V = \varphi_y$. We use the conformal mapping $\zeta = \sqrt{z}$, which maps the physical plane $z = x + iy$ with branch cut along the positive side of the real axis, corresponding to the airfoil and separated zone, onto the upper-half of the image plane, $\zeta = \xi + i\eta$ (Fig. 1). The complex conjugate velocities in the two planes are related through

$$\frac{\mathrm{d}W}{\mathrm{d}z} = \frac{\mathrm{d}W/\mathrm{d}\zeta}{\mathrm{d}z/\mathrm{d}\zeta} = \frac{1}{2\zeta}\frac{\mathrm{d}W}{\mathrm{d}\zeta}$$

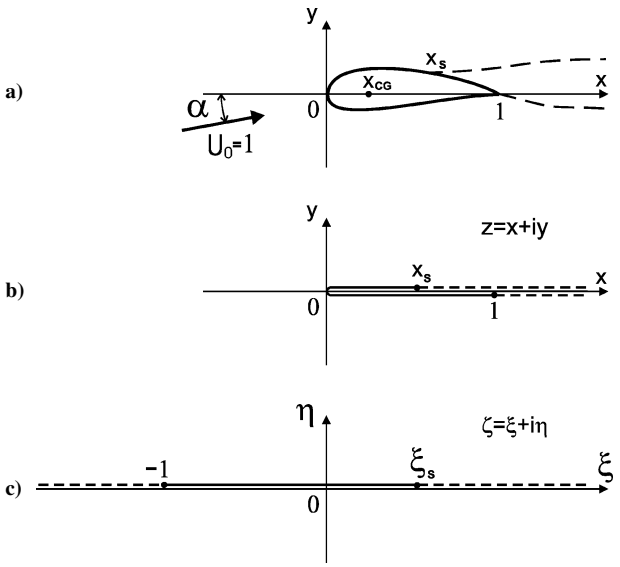

Fig. 1 Schematic for flow about a thin airfoil with upper-surface separation, in a) the linear approximation, b) the physical plane $z = x + iy$, and c) the image plane $\zeta = \xi + i\eta$.